P3.7 IMPROVING SCATTEROMETER OCEAN WIND VECTOR DATA ASSIMILATION IN ENVIRONMENT CANADA'S GLOBAL VARIATIONAL ANALYSIS AND FORECAST SYSTEM

Robert Tardif[1], Mateusz Reszka[2], Stéphane Laroche[1], Judy St-James[2]
[1]Meteorological Research Division, [2]Meteorological Service of Canada,
Environment Canada, Dorval, Canada

1. INTRODUCTION

This paper reports on activities aimed at improving the assimilation of ocean surface wind vector retrievals from scatterometers in the Canadian Global Deterministic Prediction System (GDPS). The objective is to improve global analyses and forecasts by refining the handling and interpretation of the assimilated wind observations. Prior studies have shown that the assimilation of scatterometer wind retrievals into numerical weather prediction (NWP) models provides a positive but relatively modest contribution to the overall improvement of analyses and forecasts (see Atlas et al. 2001; Leidner et al. 2003; Isaksen and Janssen 2004 among others). Among issues possibly limiting the effectiveness with which scatterometer observations are assimilated, the following can be listed:

- relatively low spatial and temporal coverage of assimilated observations;
- quality control procedures allowing the input of contaminated observations into the data assimilation system;
- artifacts of data thinning procedure;
- use of suboptimal observation error statistics;
- use of model-derived 10-m stability-dependent winds compared to scatterometer equivalent-neutral wind retrievals for the calculation of innovations;
- artifacts of methodology used for removing the inherent ambiguity of scatterometer wind vectors;
- use of static background error covariances not allowing flow-dependent propagation of information from near-surface increments to upper-level dynamics;
- characteristics of the NWP model leading to systematic errors in the background surface wind field.

In order to address some of these issues, possible avenues for improvements in the data assimilation of scatterometer winds were considered and investigated. In particular, new quality control and thinning procedures were formulated in order to eliminate ice-contaminated observations and to remove certain artifacts of the original procedure. Further tests included adjustments to the observation error variances and the adaptation of the observation operator to consider the equivalent-neutral nature of scatterometer winds. Work on assessing the impact of using flow-dependent background error statistics estimated from the operational Ensemble Kalman Filter (EnKF) system is currently ongoing, while the possible contribution from improved model physics has not yet been investigated.

* *Corresponding author address*: Dr. Robert Tardif, Meteorological Research Division, Environment Canada, 2121 Trans-Canada Highway, Dorval, Canada, H9P-1J3, E -Mail: Robert.Tardif@ec.gc.ca

2. NWP MODEL, DATA ASSIMILATION SYSTEM & SCATTEROMETER WIND OBSERVATIONS

The Canadian GDPS is composed of an incremental 4D-Var data assimilation scheme (Gauthier et al. 2007; Laroche et al. 2007), and the Global Environmental Multiscale (GEM) NWP model (Côté et al. 1998; Bélair et al. 2009). The current global configuration of the GEM model corresponds to a horizontal resolution of 33 km (exact resolution at 49°N) with 80 hybrid vertical levels (terrain-following near the surface relaxing to pressure at higher altitudes) extending from the surface to 0.1 hPa. Of direct relevance to the modeling of ocean surface winds, surface layer (SL) turbulent transfer is parameterized using the Monin-Obukhov similarity formalism, with the stability functions of Delage and Girard (1992) representing the unstable regime, and two distinct formulations for the marginally and strongly stable SLs, including an Ekman rotation of the wind vector between the surface and the top of the turbulent boundary layer height as detailed in Delage (1997).

Global analyses are generated at an interval of 6 hours by assimilating observations from various sources. Apart from scatterometers, the data assimilation system ingests observations from radiosondes and dropsondes, aircraft, land stations, buoys and ships, NOAA wind profilers, AMVs from geostationary satellites and MODIS on Aqua and Terra polar-orbiting satellites, GPS-RO and radiances from multiple channels from GOES imagers as well as from AIRS, AMSU-A and AMSU-B sensors. Analysis increments are produced on model levels at a lower horizontal resolution of 1.5°.

Over the last decade or so, scatterometer wind observations were available for assimilation from a C-band scatterometer on-board ESA's ERS-2 satellite and from the SeaWinds Ku-band rotating pencil-beam scatterometer on NASA's Quikscat satellite. Most recently, ESA's MetOp-A satellite with the ASCAT C-band scatterometer on-board (Figa-Saldaña et al. 2002) became operational. The impact of assimilating wind observations from the AMI scatterometer on ERS-2 in the Canadian NWP system was investigated by

Buehner (2002) but this data set was not adopted operationally. On the other hand, the 100-km resolution SeaWinds product provided by the Koninklijk Nederlands Meteorologisch Instituut (KNMI) was assimilated operationally from May 2008 until SeaWinds was decommissioned in November 2009.

The 25-km resolution ASCAT product provided by KNMI was introduced in the GDPS in March 2009, enabling the increase in coverage of ocean wind vector observations ingested by the assimilation system. The orbits of MetOp-A and Quikscat are complementary so that wind retrievals are available over significant portions of every ocean at every analysis time (Fig. 1). In principle, such a dual-satellite configuration provides advantages for data assimilation purposes.

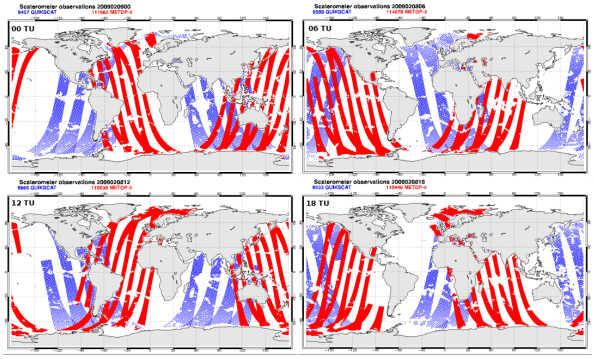

Figure 1. Example of data coverage provided by SeaWinds on Quikscat (blue) and ASCAT on MetOp-A (red), for the four analysis times of 00 UTC (upper left panel), 06 UTC (upper right), 12 UTC (lower left) and 18 UTC (lower right panel).

The implementation of ASCAT wind assimilation in the GDPS was performed using the same configuration as for the 100-km SeaWinds observations. More specifically, the same observation-error statistics are used, ambiguity removal is performed by simply selecting the wind vector solution flagged as most probable by KNMI, and wind speed cut-offs are applied at 4 m s^{-1} and 30 m s^{-1} which prevents observations outside this range from being assimilated. Quality-controlled ASCAT wind retrievals with a 25 km-resolution are obtained from KNMI and are thinned to one data point per 100 km x 100 km box. Since November 2008 retrievals are provided as equivalent-neutral winds. Following KNMI's recommendation, a value of 0.2 m s^{-1} is subtracted from the ASCAT equivalent-neutral wind product as a simple transformation to real (i.e. stability-dependent) winds. The 10-m winds diagnosed on the model grid using Monin-Obukhov similarity relations and horizontally interpolated to the observation locations are used in the calculation of innovations, or O-F values (i.e. observation minus 6-hour model forecast).

Trial assimilation cycles showed that the addition of ASCAT observations provided a slight positive impact on forecasts (not shown). More importantly, the introduction of ASCAT observations into the operational system proved especially timely due to the subsequent failure of the SeaWinds instrument.

3. RECENT MODIFICATIONS TO SCATTEROMETER DATA ASSIMILATION

For this study, the baseline configuration of the assimilation system was as outlined in the previous section, including the assimilation of SeaWinds and ASCAT observations. Modifications to various aspects of this baseline system were investigated, with the intent of improving the impact of scatterometer wind observations in the GDPS. Specific investigations were carried out on the basis of assimilation experiments using the 3D-Var FGAT (First-Guess at Appropriate Time) assimilation scheme to minimize the computational requirements, allowing more experiments to be performed. Results from these experiments are outlined below.

3.1. Quality control & data thinning

Observations considered for assimilation undergo checks to ensure their quality. Specific to scatterometer wind observations, contamination by rain is a main concern, particularly for Ku-band (SeaWinds) observations, while contamination by the presence of sea ice within the footprint of the instrument affects wind retrievals from both Ku-band and C-band (ERS-2 and ASCAT) scatterometers. The extensive quality control performed by the data provider (KNMI) is relied upon for simplicity. Only the observations that have not been flagged as suspect by KNMI are considered for assimilation into the GDPS.

As mentioned previously, during the thinning procedure wind retrievals with a speed below 4 m s^{-1} and above 30 m s^{-1} are eliminated since the retrievals are known to be less accurate in very weak and very strong wind conditions. Quality-controlled SeaWinds observations from the 100-km data stream are used as-is, while the 25-km ASCAT product is thinned by selecting those observations which are closest to the nodes of a prescribed 100 km x 100 km global grid. Finally, a background-check and variational quality control are performed during the assimilation process to further eliminate remaining observations that show large discrepancies with respect to the model background field.

Long-term monitoring of ASCAT data had revealed rather conspicuous bands of large O-F errors along the edge of sea ice in both hemispheres (Fig. 2). The presence of ice undoubtedly influences radar backscatter which in turn affects results in an adverse way when backscatter is interpreted in a context of ocean surface wind retrieval. It is noteworthy that these O-F outliers did not occur for SeaWinds data (indeed, KNMI employed a more stringent ice-contamination check with SeaWinds than with ASCAT).

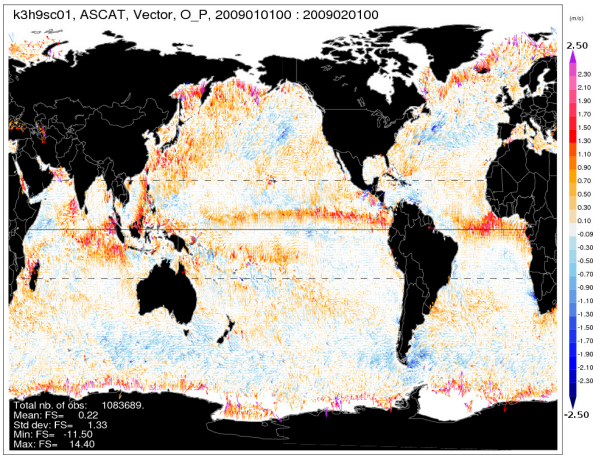

Figure 2. Map of the monthly averaged O-F vectors for the 10-metre wind with respect to ASCAT observations, over January 2009. The color scale represents the difference in wind speed (m s^{-1}).

As part of an experiment, the quality control routine was modified to eliminate ASCAT data within a given distance of sea ice by mapping the observations to the operational Canadian Meteorological Center (CMC) ice analysis. A conservative distance of 550 km was adopted, which ensures that virtually all of the contaminated data are removed. This modification has the effect of eliminating a significant fraction (about 10%) of the original retrievals, and it is planned that smaller threshold distances will be investigated in the future. Additionally, with ASCAT, it was found that a disproportionately high number of measurements at the edges of the satellite swaths and near the low-speed cut-off passed the background check (a consequence of the track geometry and subsequent thinning). Since these data tend to be associated with somewhat larger O-F errors, the thinning procedure was generalized to account for this artifact.

In order to assess the above modifications, 3D-Var FGAT assimilation cycles were performed for the period Dec 15 2008 – Jan 31 2009 using data processed by the operational (control) and modified (experiment) quality control routines. It was subsequently verified that the O-F outliers in the vicinity of sea ice were practically eliminated and that overall O-F statistics decreased, albeit by a modest amount. For example, Figure 3 shows the time-mean standard deviation of the O-F error associated with the wind direction, as diagnosed from both cycles. The error is plotted as a function of the wind vector cell (WVC), i.e. the cross-track position, where WVCs 1-21 and 22-42 respectively correspond to the two swaths of the ASCAT instrument. The shade of green (dark to light) shows the relative range (lowest to highest) of the number of assimilated observations per WVC. Clearly the overall amplitude of the standard deviation is reduced in the experimental cycle, and the assimilated observations are more evenly distributed across the track.

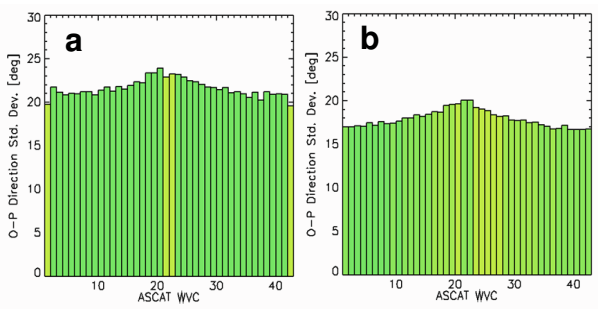

Figure 3. O-F standard deviation over January 2009 for the 10-m wind direction as a function of wind vector cell (WVC) obtained from the control (a) and experimental (b) cycles (see text).

Five-day forecasts were launched from the control and experimental analyses every 12 hours (86 forecasts per cycle) and verification statistics were computed against radiosonde observations as well as against the analyses themselves (not shown). A significant decrease in scores was observed over North America at a lead time of five days, particularly in the height field, as shown in Figure 4. Verification against analysis (not shown) suggests an improvement in forecasts over North America at two days and over the Northern Hemisphere at five days. These and other diagnostics seem to indicate that removal of the ice-contaminated observations along the east and west coasts of North

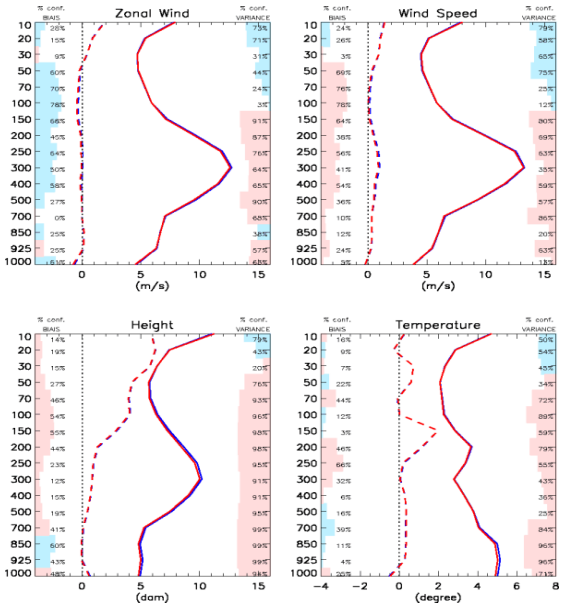

Figure 4. Forecast verification scores against the radiosonde network at 120 hours over North America for the (blue) control cycle and (red) experimental cycle with improved sea-ice screening and data thinning. The dashed lines indicate the mean forecast error (bias) while the solid lines represent the standard deviation of errors. Corresponding significance levels are indicated by colored boxes on the left and right sides of each plot.

America has a beneficial influence on forecast skill. Somewhat surprisingly, the impact is negligible in other regions of the globe, at least during this assimilation period. It remains unknown, for example, if the beneficial effect would shift to the Southern Hemisphere under June/July conditions.

3.2. Adjustments to the observation error variance

In the baseline configuration, the observation error for scatterometer data is specified as a single value for both zonal (U) and meridional (V) wind components, and applied globally. The prescribed standard deviation for both SeaWinds and ASCAT is 1.7 m s^{-1} which is similar to values used in the ECMWF forecast system (IFS Documentation, 2008). Desroziers et al. (2005) suggest a method for re-estimating the observation error based on O-F information from previous assimilation cycles in order to obtain values more consistent with the other statistics used. When the suggested calculation is applied to the cycles described in the previous section, it yields standard deviations of approximately 1.0 and 1.1 m s^{-1} for U and V, respectively.

Treating the experimental cycle in the last section as the control, a new cycle was performed for the period Dec. 15 2008 – Jan. 31 2009 with the re-estimated observation errors. As before, five-day forecasts were launched from both sets of analyses, followed by verification tests. A positive impact on forecast skill was obtained over the Northern Hemisphere for lead times of five days, as suggested by the scores against radiosondes plotted in Figure 5.

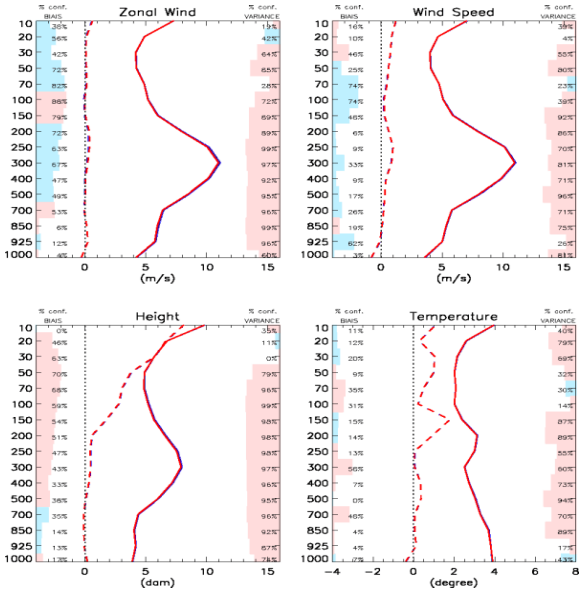

Figure 5. Forecast verification scores against the radiosonde network at 120 hours in the Northern Hemisphere for the (blue) control cycle and (red) experimental cycle with reduced observation error variance. The control cycle in this figure is the experimental cycle in Figure 4.

Most of this effect can be attributed to improved forecasts over North America, whereas the influence is negligible in other geographic regions. Scores against analysis (not shown) demonstrate a similar behavior, in that the largest effect seems to be improved forecasts over North America for lead times of three to five days. The signal is apparent in the Northern Hemisphere, particularly at day-4.

It was also found that the decreased observation error resulted in an overall reduction in O-F statistics (not shown), which seems to indicate a better synergy between the model and observations. One can easily conclude from these experiments that information from the scatterometer measurements is transmitted upward and has a significant effect at least as high as the upper troposphere. Indeed, the greatest impact of these observations tends to occur not at the surface but at higher altitudes. It is also apparent that the scatterometer data generally have a positive effect on forecast skill, presumably by correcting biases inherent in the analysis/forecast system.

3.3. Assimilation of observations as equivalent-neutral winds

Scatterometer winds are derived from the observed ocean surface radar backscatter using empirical Geophysical Model Functions (GMF). The GMF traditionally used to estimate wind retrievals from SeaWinds was calibrated against equivalent-neutral winds (Wentz and Smith 1999), as is the case for ASCAT winds provided by KNMI since November 2008 (Hersbach 2010). Equivalent-neutral winds are defined as the wind speed calculated from the stress and roughness length consistent with the observed atmospheric stratification but neglecting the effect of stability in the expression of the modified log-wind profile (Ross et al. 1985; Liu and Tang 1996). The usual stability-dependent wind profile is expressed as

$$\mathbf{u}(z) = \frac{\mathbf{u}_*}{k}\left[\ln\left(\frac{z}{z_{0m}}+1\right)+\psi_m\left(\frac{z+z_{0m}}{L}\right)-\psi_m\left(\frac{z_{0m}}{L}\right)\right] \quad (1)$$

whereas the equivalent-neutral profile is obtained using

$$\mathbf{u}_{en} = \frac{\mathbf{u}_*}{k}\ln\left(\frac{z}{z_{0m}}+1\right), \quad (2)$$

where $\mathbf{u}_*$ is the friction velocity vector, z_{0m} is the momentum roughness length, k is the von Karman constant, ψ_m is the Monin-Obukhov stability function for momentum and L is the Obukhov length. A global average difference of +0.2 m s^{-1} between equivalent-neutral and stability-dependent winds (equivalent-neutral stronger than stability-dependent winds) has been obtained by Portabella and Stoffelen (2009). This subtlety in the definition of scatterometer winds has been largely ignored until recently in the data

assimilation of ocean surface winds. Innovations (e. g. O-F values) were typically calculated using the model-diagnosed 10-m stability-dependent wind following the methodology described in Geleyn (1988). The consequence for scatterometer data assimilation is a complete neglect of the variability in the difference between stability-dependent and equivalent-neutral 10-m winds in the calculation of innovations. Deviations from the +0.2 m s^{-1} global average are found to be dependent on ambient conditions, possibly reaching an order of magnitude of about 1 m s^{-1} depending on wind speed and static stability conditions (Fig. 6). This translates into areas with significant departures from the +0.2 m s^{-1} value. Such areas were found to cover significant portions of the global ocean in January 2009 (Fig. 7). Larger positive values were located off the eastern seaboard of North America associated with unstable boundary layer conditions from the outflow of cold continental air over the Gulf Stream and open waters of the Labrador Sea, while negative values associated with stable conditions characterized a large area of the northeastern Pacific where southerly flows prevailed. Other large areas with negative differences were found in the Southern Ocean north of Antarctica's Murdoch Sound and over and east of the Drake Passage. Large positive differences interspersed with negative values were found the indo-Pacific warm pool. As reported by Kara et al. (2008) and Hersbach (2010), the location and extent of such areas in the extra-tropical regions depend on the seasonally varying low-level flow regimes and temperature contrasts between the low-level air and the sea surface temperature.

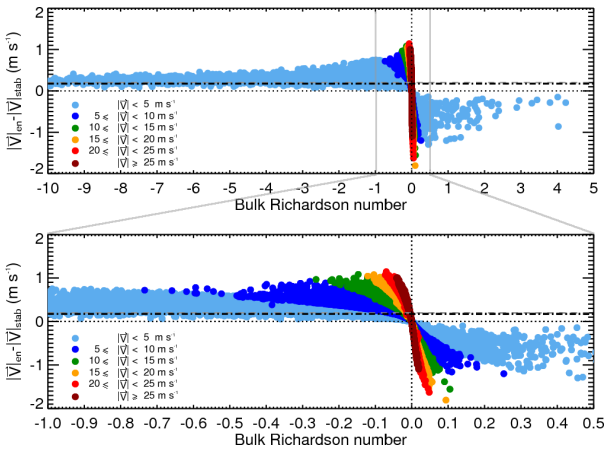

Figure 6. Difference between 10-m equivalent-neutral and stability-dependent wind speed (in m s^{-1}) as a function of the bulk Richardson number, calculated at from GEM model output at the locations of available scatterometer observations during January 2009. The bottom frame provides a close-up view of conditions closer to neutral stratification. The dashed line represents the average value of +0.2 m s^{-1}.

To fully represent this variability in the model background, an equivalent-neutral wind observation operator was designed and implemented in the assimilation system. Corresponding analyses and related forecasts are compared with those produced with the baseline system, where innovations are calculated on the basis of 10-m stability-dependent winds interpolated to the location of observations, and scatterometer winds corrected to real (i.e. stability-dependent) winds by applying a -0.2 m s^{-1} correction.

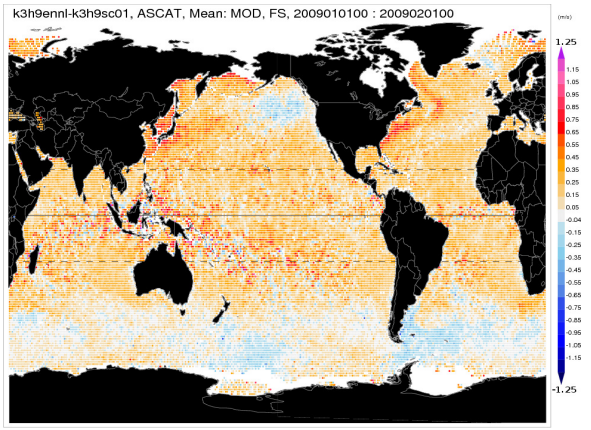

Figure 7. Map of the monthly average difference between the model background 10-m equivalent-neutral and stability-dependent wind speed (in m s^{-1}) over 1°x1° latitude-longitude grid boxes for January 2009.

With the new observation operator, the background state is first interpolated from model grid points to the location of the observations, with the 10-m equivalent-neutral wind then calculated at every observation point using Eq. (2), where the friction velocity is calculated locally using

$$\mathbf{u}_* = \frac{k\mathbf{u}(z_M)}{\ln\left(\frac{z_M}{z_{0m}}+1\right)+\psi_m\left(\frac{z_M+z_{0m}}{L}\right)-\psi_m\left(\frac{z_{0m}}{L}\right)}, \qquad (3)$$

where $\mathbf{u}(z_M)$ is the interpolated model wind vector at the lowest prognostic level located at height z_M. The momentum roughness length z_{0m} over the oceans is evaluated using the well-known Charnock formulation (Charnock 1955)

$$z_{0m} = 0.018\frac{|\mathbf{u}_*|^2}{g}. \qquad (4)$$

The preliminary version of the equivalent-neutral wind operator is based on the same TL/AD as in the baseline system (i.e. bilinear interpolation operator). Therefore any differences in the analyses and forecasts compared to results from the baseline system are solely related to the change in the calculation of innovations.

Month-long trial assimilation cycles were performed over the period of January 2009 using the 3D-Var FGAT assimilation scheme. Both SeaWinds and ASCAT winds are assimilated. The control cycle is based on the baseline configuration while the experimental cycle uses the innovations calculated with the equivalent-neutral observation operator. All other aspects of the data assimilation are identical in the two cycles.

The $1^{o}x1^{o}$ monthly-averaged differences in 10-m wind innovations with respect to ASCAT observations between the two experiments are shown in Figure 8. The global average difference is equal to zero as expected, but significant regional differences are noticeable and correspond to the highlighted regions of larger differences between equivalent-neutral and stability-dependent background winds shown in Fig. 7. The perceived overestimation of wind speeds by the model (negative O-F) over stably stratified areas in the southern ocean in the control cycle (see Figs. 2 and 7) is partially alleviated when equivalent-neutral innovations are considered. In contrast, the overestimation of wind speeds by the model in the control experiment over the Gulf Stream (area of negative O-F values off the east coast of the US in Fig. 2) is further enhanced when the equivalent-neutral operator is used. The stronger equivalent-neutral winds in the unstable Gulf Stream surface layer (larger positive values over the same area in Fig. 7) lead to stronger negative innovations (negative values of innovation differences off the US northeastern coast in Fig. 8).

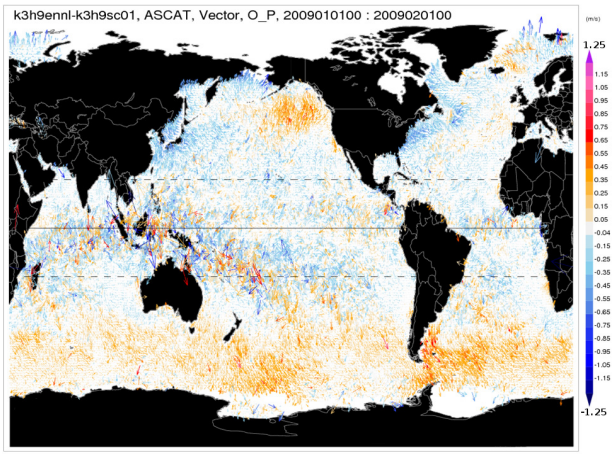

Figure 8. Map of the monthly averaged (January 2009) difference in 10-metre wind vector innovations with respect to ASCAT observations between the cycles performed with the baseline system (control) and with the equivalent-neutral observation operator (experiment). The color scale represents the difference in wind speed (in m s^{-1}).

Differences in innovations lead to different increments in near-surface wind as well as for other correlated variable as determined from background error covariances. Figure 9 illustrates the average differences in the resulting analyses for near-surface wind speed (top frame) and the geopotential at 1000 hPa (proxy for surface pressure) (bottom frame). Stronger analyzed winds were produced over most of the southern ocean in the analyses produced using the equivalent-neutral observation operator. This is particularly the case for areas where significantly weaker equivalent-neutral versus stability-dependent winds were diagnosed compared to the +0.2 m s^{-1} global correction (e.g. negative values in Fig. 7). In comparison, weaker winds were analyzed over the Gulf Stream, Labrador Sea and over a large portion of the western Pacific off of Japan with the new observation operator. In turn, differences in surface wind increments are associated with differences in increments in the mass field, as indicated by the average difference of the analyzed geopotential field at 1000 hPa (bottom frame of Fig. 9). An acceleration of the wind of a few tenths of meters per second over the southern ocean in the experimental analyses is associated with a band of lower geopotential heights (lower surface pressure up to 1 hPa) to the south along the coast of Antarctica and areas of higher geopotential heights (higher surface pressure of similar magnitude) over the northern portion

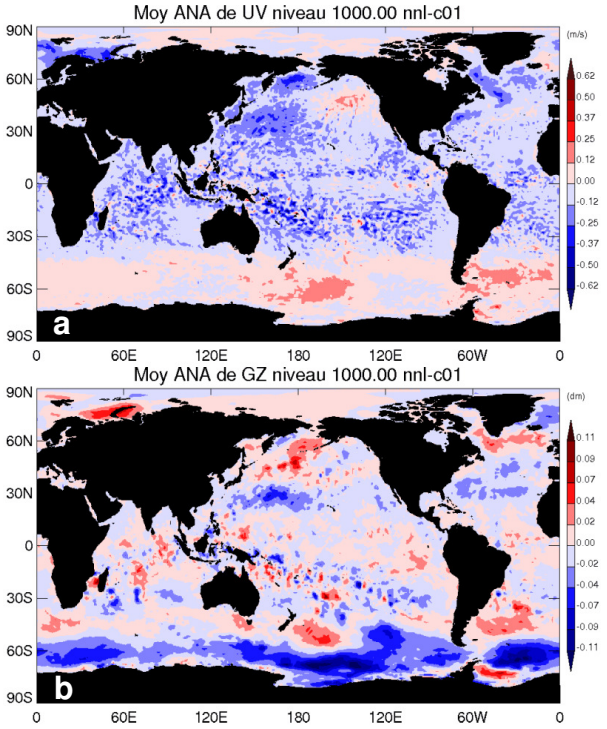

Figure 9. Monthly averaged differences in near-surface wind speed in m s^{-1} (a) and geopotential height in decameters at 1000 hPa (b), for analyses obtained by using the equivalent-neutral observation operator versus using the classic 10-m stability-dependent wind diagnostic, for January 2009.

of the southern ocean cyclone track. Similar features can also be observed in the northern hemisphere, with areas of lower pressure in the western Pacific south of

the Kuroshio extension and higher surface pressure north of the extension, and lower pressures over the mid-Atlantic in association with higher surface pressure over the north Atlantic, just south of Greenland and Iceland.

The use of an observation operator fully taking into account the equivalent-neutral nature of scatterometer winds in the calculation of innovations therefore leads to noticeable but relatively modest changes in the resulting analyses. To fully assess the impact of these changes, 5-day forecasts issued from the control and experimental analyses produced at 0000 UTC and 1200 UTC during January 2009 are compared. The corresponding verification statistics against radiosondes over North America are shown in Figure 10. Forecast biases are for the most part unaffected by the use of the new observation operator, however slight but statistically significant reductions of the error standard deviation are obtained in the experimental forecasts for the wind around 100-200 hPa, over most of the troposphere for the geopotential height and in the lower troposphere for temperature with respect to the global radiosonde dataset (not shown). Such improvements only begin to appear for forecast horizons of 4 days and beyond. Thus, a simple modification of the observation operator to improve the representation of the equivalent-neutral definition of scatterometer winds provides noticeable improvements in medium-range forecasts.

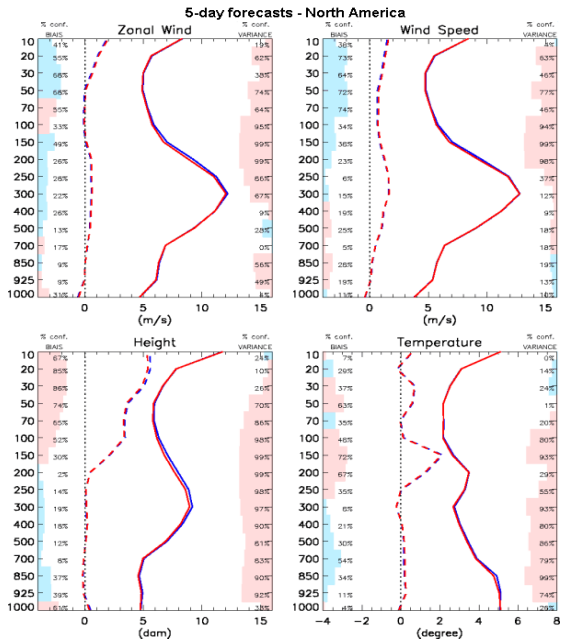

Figure 10. Forecast verification scores against radiosondes over North America, at 120 hours from analyses produced from the control cycle (blue) and from the experiment with the equivalent-neutral observation operator (red),. Significance levels are indicated by colored boxes on the left and right sides of each plot, corresponding to the bias (dashed lines) and standard deviation, (solid lines) respectively.

4. SUMMARY AND OUTLOOK

Some issues possibly limiting the effectiveness with which scatterometer observations are assimilated, were identified and related modifications were investigated. Individual changes to the assimilation system have all led to modest but significant changes in the analyses and have proven beneficial in terms of forecast skill of the NWP system. Interestingly, the impact of the modifications affecting the assimilation of ocean surface wind observations is more prevalent aloft rather than near the surface, and characterizes the medium-range forecasts in all the experiments presented herein. This seems to suggest that improvements in scatterometer data assimilation contribute at better constraining the larger scales driving the global circulation. A better understanding of this specific role of scatterometer winds however requires further investigation.

With respect to ongoing and future work, results from individual investigations have been presented on the basis of 3D-Var FGAT cycles, showing individual benefits for one month during boreal winter. Efforts toward integrating the various improvements and assessing the combined benefit in full 4D-Var experiments will soon be undertaken, including a test period during boreal summer.

Additional ongoing efforts include the investigation of other issues listed in section 1 not considered by the present work. For instance, scatterometer measurements are inherently associated with a directional ambiguity, and retrieval algorithms typically provide two or four possible solution vectors for each observation. The solution used in the CMC operational assimilation system is the one flagged as most likely by KNMI. However, since the selection procedure adopted at KNMI relies on a comparison with ECMWF wind forecasts, the internal consistency of the GDPS assimilation system may be improved if this step is performed as part of the background check. Preliminary calculations have suggested that this modification does not offer a significant benefit in terms of reducing mean O-F statistics. However these calculations were performed on trial fields from an existing cycle, and did not account for the feed-back which occurs between the model and analysis scheme. Moreover, the investigation was performed for ASCAT data which contained two possible solutions, whereas the KNMI product has been recently upgraded to contain four solutions. It is planned that the addition of ambiguity removal to the background check routine will be tested in the near future. For a robust result, the experiment configuration should include the ice-detection and quality control modifications discussed above.

Another avenue of research with regard to scatterometer data assimilation is the use of flow-dependent background-error statistics. The GDPS currently makes use of variances and covariances derived using the NMC method. Because these statistics are static over each month and have no zonal dependence, they are not reflective of the instantaneous meteorological state of the atmosphere at any given

assimilation time. Of chief importance for scatterometer observations, and surface winds in general, are the covariances due to the Ekman pumping mechanism, which has a significant effect on divergence in the boundary layer. Current efforts are aimed at estimating the three-dimensional structure of the divergence field at every assimilation time based on ensembles of 6-hour forecasts, which are available operationally as part of the CMC Ensemble Kalman Filter assimilation system.

Other efforts deal with the development and testing of the complete tangent linear and adjoint of the equivalent-neutral observation operator to assess the impact of using more sophisticated formulations in the minimization of the cost function and resulting analyses.

Acknowledgments

Funding for this research has been provided by the Canadian Search And Rescue New Initiatives Fund (SAR NIF).

REFERENCES

Atlas, R., R, N. Hoffman, S. M. Leidner, J. Sienkiewicz, T.-W. Yu, S. C. Bloom, E. Brin, J. Ardizzone, J. Terry, D. Bungato, and J. C. Busem, 2001: The effects of marine winds from scatterometer data on weather analysis and forecasting. *Bull. Amer. Meteorol. Soc.*, **82**, 1965–1990.

Bélair, S., M. Roch, A.-M. Leduc, P. Vaillancourt, S. Laroche and J. Mailhot, 2009: Medium-range quantitative precipitation forecasts from Canada's new 33-km deterministic global operational system. Wea. Forecasting, **24**, 690–708.

Buehner, M., 2002: Assimilation of ERS-2 scatterometer winds using the Canadian 3D-var. *Atmos.-Ocean,* **40**, 361-376.

Charnock, H., 1955: Wind stress over a water surface. *Quart. J. Roy. Meteor. Soc.*, **81**, 639-640.

Côté, J., S. Gravel, A. Méthot, A. Patoine, M. Roch, and A. Staniforth, 1998a: The operational CMC-MRB Global Environmental Multiscale (GEM) model: Part I - Design considerations and formulation. *Mon. Wea. Rev.*, **126**, 1373-1395.

Delage, Y. and C. Girard, 1992: Stability functions correct at the free convection limit and consistent for both the surface and Ekman layers. *Bound.-Layer Meteor.*, **58**, 19-31.

Delage, Y., 1997: Parameterising sub-grid scale vertical transport in atmospheric models under statically stable conditions. *Bound.-Layer Meteor.*, **82**, 23-48.

Desroziers, G., L. Berre, B. Chapnik and P. Poli, 2005: Diagnosis of observation, background and analysis-error statistics in observation space. *Quart. J. Roy. Meteor. Soc.,* **131**, 3385–3396.

Figa-Saldaña, J., J. J. W. Wilson, E. Attema, R. Gelsthorpe, M. Drinkwater, and A. Stoffelen, 2002: The advanced scatterometer (ASCAT) on the meteorological operational (MetOp) platform: A follow on for European wind scatterometers. *Can. J. Remote Sens.*, **28**, 404–412.

Gauthier, P., M. Tanguay, S. Laroche, S. Pellerin and J. Morneau, 2007: Extension of 3D-Var to 4D-Var: Implementation of 4D-Var at the Meteorological Service of Canada. *Mon. Wea. Rev.*, **135**, 2339–2354.

Geleyn, J.-F., 1988: Interpolation of wind, temperature and humidity values from model levels to the height of measurement. *Tellus*, **40A**, 347-351.

Hersbach, H., 2010: Comparison of C-band scatterometer CMOD5.N equivalent neutral winds with ECMWF. *J. Atmos. Oceanic Technol.*, **27**, 721-736.

IFS Documentation–CY33r1. ECMWF technical manual. available at: http://www.ecmwf.int/research/ifsdocs/CY33r1/ASSIMILATION/IFSPart2.pdf

Isaksen, L., and P. A. E. M. Janssen, 2004: The benefit of ERS scatterometer winds in ECMWF's variational assimilation system. *Quart. J. Roy. Meteor. Soc.*, **130**, 1793–1814.

Kara, A. B., A. J. Wallcraft, and M. A. Bourassa, 2008: Air-sea stability effects on the 10 m winds over the global ocean: Evaluations of air-sea flux algorithms, *J. Geophys. Res.*, **113**, C04009, doi:10.1029/2007JC004324.

Laroche, S., P. Gauthier, M. Tanguay and S. Pellerin, 2007: Impact of the different components of 4D-Var on the global forecast system of the Meteorological Service of Canada. *Mon. Wea. Rev.*, **135**, 2355-2364.

Leidner, S. M., L. Isaksen, and R. N. Hoffman, 2003: Impact of NSCAT winds on tropical cyclones in the ECMWF 4D-Var assimilation system, *Mon. Wea. Rev.*, **131**, 3–26.

Liu, W. T. and W. Tang, 1996: *Equivalent Neutral Wind*. JPL Publication 96-17, Jet Propulsion Laboratory, Pasadena, 16 pp.

Portabella, M., and A. Stoffelen, 2009: On scatterometer ocean stress. *J. Atmos. Oceanic Technol.*, **26**, 368-382.

Ross, D.B., V.J. Cardone, J. Overland, R. D. McPherson, W. J. Pierson Jr., and T. Yu, 1985: Oceanic surface winds. *Adv. Geophys.*, **27**, 101–138.

Wentz, F. J., and D. K. Smith, 1999: A model function for the ocean normalized radar cross section at 14 GHz derived from NSCAT observations, *J. Geophys. Res.*, **104**(C5), 11499–11514.